Peroxodiferric Intermediate of Stearoyl-Acyl Carrier Protein Δ^9 Desaturase: Oxidase Reactivity during Single Turnover and Implications for the Mechanism of Desaturation†

John A. Broadwater,‡,§ Jingyuan Ai,|| Thomas M. Loehr,|| Joann Sanders-Loehr,|| and Brian G. Fox*,§

The Institute for Enzyme Research, Graduate School, University of Wisconsin, Madison, Wisconsin 53705, Department of Biochemistry, College of Agricultural and Life Sciences, University of Wisconsin, Madison, Wisconsin 53706, and The Department of Biochemistry and Molecular Biology, Oregon Graduate Institute of Science and Technology, Portland, Oregon 97291-1000

Received July 31, 1998; Revised Manuscript Received August 31, 1998

ABSTRACT: Combined optical and resonance Raman studies have revealed the formation of an O_2-adduct upon exposure of $4e^-$ chemically reduced stearoyl-acyl carrier protein Δ^9 desaturase to stearoyl-ACP and 1 atm O_2. The observed intermediate has a broad absorption band at 700 nm and is remarkably stable at room temperature ($t_{1/2} \approx 26$ min). Resonance Raman studies using $^{16}O_2$ gas reveal vibrational features of a bound peroxide [ν_s(Fe−O_2), 442 cm^{-1}; ν_{as}(Fe−O_2), 490 cm^{-1}; ν(O−O), 898 cm^{-1}] that undergo the expected mass-dependent shifts when prepared in $^{16}O^{18}O$ or $^{18}O_2$. The appearance of two Fe−O_2 vibrations, each having a single peak of intermediate frequency with $^{16}O^{18}O$, proves that the peroxide is bound symmetrically between the two iron atoms in a μ-1,2 configuration. The same results have been obtained in the accompanying resonance Raman study of ribonucleotide reductase isoform W48F/D84E [P. Moënne-Loccoz, J. Baldwin, B. A. Ley, T. M. Loehr, and J. M. Bollinger, Jr. (1998) *Biochemistry 37*, 14659−14663], thus making it likely that other members of the class II diiron enzymes form related peroxodiferric intermediates. Study of the reactivity of peroxodiferric Δ9D revealed that this intermediate underwent $2e^-$ reduction leading to an oxidase reaction and recovery of the resting ferric homodimer. In contrast, biological reduction of the same enzyme preparations using ferredoxin reductase and [2Fe-2S] ferredoxin gave catalytic desaturation with a turnover number of 20−30 min^{-1}. The profound difference in catalytic outcome for chemically and enzymatically reduced Δ9D suggests that redox-state dependent conformational changes cause partition of reactivity between desaturase and oxidase chemistries. The Δ9D oxidase reaction represents a new type of reactivity for the acyl-ACP desaturases and provides a two-step catalytic precedent for the "alternative oxidase" activity recently proposed for a membrane diiron enzyme in plants and trypanosomes.

Enzymes containing oxo- or hydroxo- and carboxylato-bridged diiron sites are a functionally and structurally diverse group (*1*−*3*). Sequence alignments, catalytic properties, spectroscopic studies, and crystal structures support the division of this group into at least three, and perhaps four, different classes (*4*−*8*). The class II diiron enzymes include ribonucleotide reductase, RNR R2[1] (*9*), bacterial hydrocarbon monooxygenases (*10*, *11*), and acyl-ACP desaturases (*12*). These enzymes have a similar protein fold that contains two copies of the amino acid sequence (Asp/Glu)$X_{\sim 40}$GluXXHis separated by ∼100 amino acids, and catalyze O_2 activation as part of their respective reaction cycles. Although the protein folds are different, ferritins (*7*) and rubrerythrin (*8*) also contain diiron centers that are closely related to the other class II diiron enzymes, and catalyze O_2 activation as part of the ferroxidase reaction (*13*, *14*).

Stearoyl-ACP Δ^9-desaturase (Δ9D) is the best characterized acyl-ACP desaturase (*15*). This soluble, homodimeric enzyme ($M_r \approx 84$ kDa) catalyzes the NAD(P)H- and O_2-dependent introduction of a cis double bond between carbons 9 and 10 of stearoyl-ACP (18:0-ACP), yielding oleoyl-ACP (18:1-ACP) with a turnover number of 20−30 min^{-1}. Optical, Mössbauer (*16*), RR (*4*), and EXAFS (*17*) studies have shown that resting Δ9D contains 4 mol of iron in two oxo-bridged diferric centers, while an X-ray structure revealed that $4e^-$ reduced Δ9D produced by photoreduction had lost the oxo bridge (*12*). Furthermore, RR studies of azidoΔ9D revealed a μ-1,3 bridged species and the absence of the oxo bridge (*18*), which suggested that a μ-1,2 peroxy intermediate could be formed during Δ9D catalysis. The structural variations revealed by these[2] and related studies

† This work was supported by grants from the NIH (GM-50853 to B.G.F. and GM-18865 to J.S.L. and T.M.L.). B.G.F. is a Shaw Scientist of the Milwaukee Foundation (1994−1999).

* To whom correspondence should be addressed. E-mail: fox@enzyme.wisc.edu. Phone: (608) 262-9708.

‡ Trainee of the Graduate Training Grant in Molecular Biophysics.

§ University of Wisconsin—Madison.

|| Oregon Graduate Institute of Science and Technology.

[1] Abbreviations: ACP, acyl carrier protein; 18:0-ACP, stearoyl-ACP; 18:1-ACP, oleoyl-ACP; Δ9D, 18:0-ACP Δ^9 desaturase; resting Δ9D, form of Δ9D containing all ferric sites; $4e^-$ Δ9D, chemically reduced form of Δ9D containing all ferrous sites; MMOH, hydroxylase component of methane monooxygenase; RNR R2, iron-containing component of ribonucleotide diphosphate reductase; RR, resonance Raman.

10.1021/bi981839i CCC: $15.00
Published on Web 10/02/1998

of other diiron enzymes (*10, 11, 19*) suggest substantial flexibility in the carboxylate ligands (*20*).

The ability of the carboxylate ligands to permit rearrangements at the metal center concomitant with changes in redox state has emerged as a consistent feature of the proposed catalytic mechanisms of diiron enzymes (*10, 18*−*23*). Furthermore, reaction intermediates (*24*) including peroxodiferric (*13, 25*−*27*), bis-μ-oxo diiron(IV) (*21, 27, 28*), and ferric-ferryl mixed valence (*29*−*32*) have been recently identified. The previous paper in this issue describes the RR characterization of a peroxodiferric intermediate of RNR R2 isoform W48F/D84E (*26*). The vibrational data clearly demonstrate that this intermediate has a symmetric μ-1,2 structure, while other work has shown that the corresponding intermediate observed in the related RNR R2 isoform D84E decays with $k' \approx 0.59-0.93$ s^{-1} to the yield the natural product, a radical at Y122 (*25*).

In this work, optical, RR, and catalytic studies of both biologically and chemically reduced Δ9D are reported. During multiple turnover, a biological electron-transfer chain consisting of ferredoxin reductase and [2Fe-2S] ferredoxin is required to introduce minimally 2e$^-$ to the resting ferric enzyme. No evidence for a mixed valence [Fe(II)Fe(III)] state has been obtained from either Mössbauer or EPR studies, suggesting that the biological electron-transfer chain will give 2e$^-$ reduction of one diferric center of the resting enzyme to yield the diferrous state, while the other diiron center will remain in the diferric state. In contrast, chemical reduction produces an enzyme containing all ferrous sites as shown by Mössbauer spectroscopy (*16*), which will herein be called 4e$^-$ Δ9D. The present work reveals that 4e$^-$ Δ9D can form a symmetric μ-1,2 peroxodiferric intermediate whose structure is remarkably similar to that of RNR R2 D84E (*25*) and W48F/D84E (*26*). However, the Δ9D intermediate, which has only been detected by starting the reaction with 4e$^-$ Δ9D, 18:0-ACP, and O_2, decays via an unanticipated 2e$^-$ reduction of the peroxodiferric center (or a subsequent, undetected intermediate derived from this species) to restore the resting, completely ferric enzyme. The overall stoichiometry, $O_2 + 4e^- + 4H^+ \rightarrow 2H_2O$, corresponds to an oxidase reaction, which represents a new mode of catalysis for the diiron desaturases.

MATERIALS AND METHODS

Sample Preparations. Δ9D was obtained as previously described (*33*), the protein concentration was determined by dye binding (*34*), and the iron content was determined by complexation with tripyridyl-*S*-triazine (*35*). Spinach holo-ACP isoform I (>95% phosphopantetheinylation) was produced by coexpressing a synthesized gene composed of codons favored for high-level expression in *Escherichia coli* with the gene for *E. coli* holo-ACP synthase (*36*). Holo-ACP was converted to 18:0-ACP (>95%) using *E. coli* acyl-ACP synthase (*37*) modified to contain a C-terminal His_6 tag. Holo- and acyl-ACP were quantitated by reaction of Ellman's reagent with the phosphopantetheine thiol group of either holo-ACP or holo-ACP formed by treating acyl-ACP with NH_2OH. Further details of the ACP preparations will be reported elsewhere. Reduction of anaerobic solutions of Δ9D was accomplished by titration with concentrated solutions of buffered sodium dithionite (*16*). After reduction, anaerobic 18:0-ACP was added, and then the headspace of the anaerobic cuvette was replaced with O_2 (1 atm). Samples for Raman spectroscopy were also prepared with $^{16}O^{18}O$ (50 atom % ^{18}O, ICON, Summit, NJ) and $^{18}O_2$ (98 atom % ^{18}O, ICON). Raman analysis of the $^{16}O^{18}O$ gas showed the expected distribution of 25% $^{16}O_2$, 50% $^{16}O^{18}O$, and 25% $^{18}O_2$. Samples were frozen in liquid nitrogen immediately after preparation, and Raman spectra were obtained at room temperature within 10 min.

Spectroscopic Measurements. Optical spectra were obtained using a Hewlett-Packard 8452 diode array spectrometer at 20 °C. The rate of decay of peroxodiferric Δ9D was determined by nonlinear least-squares fitting using the equation $A(t) = A(0)\exp(-k_{app}t) + A_\infty$. A_∞ was determined by Kedzy-Swinbourne analysis (*38*). RR spectra were obtained using a custom McPherson 2061 spectrograph (0.67 m, 1800 groove grating) using a Kaiser Optical holographic super-notch filter with a Princeton Instruments liquid N_2-cooled (LN-1100PB) CCD detector with 3 cm^{-1} spectral resolution. Excitation at 647.1 nm (40 mW) was provided by a Coherent Innova 302 Kr laser. All spectra were collected using a 90° scattering geometry on samples in capillaries cooled by N_2 gas that had been passed through an ice bath. Absolute frequencies were obtained by calibration with aspirin and CCl_4 and are accurate to ±1 cm^{-1}. Isotope shifts, obtained from spectra recorded under identical experimental conditions, were evaluated by abscissa expansion and curve resolution of overlapping bands and are accurate to ±0.5 cm^{-1}.

Product Determinations. Multiple turnover desaturation reactions were performed at 20 °C in Teflon-sealed vials containing 250 μL of 50 mM HEPES buffer, pH 7.8, 50 mM NaCl, 50 nmol of 18:0-ACP, 0.5 nmol of Δ9D, 2 nmol of *Anabaena* 7120 vegetative ferredoxin, 1.5 nmol of ferredoxin NADPH oxidoreductase, and 600 nmol of NADPH. After either multiple or single turnover reactions, acyl thioesters were converted to acyl alcohols using sodium borohydride (*39*) and extracted with chloroform. The acyl alcohols were converted to silyl derivatives using (*N*,*O*-bis-[trimethylsilyl]acetamide) (Alltech Associates, Deerfield, IL). Silyl alcohols were quantitated by gas chromatography using an Econo-Cap SE-30 column (15 m × 0.53 mm, 1.2 μm film thickness, Alltech). The column was maintained at 200 °C, the injection port at 250 °C, and the flame ionization detector at 300 °C. Helium carrier gas flow was 2.9 mL/min. For these conditions, the following elution times were observed: stearoyl alcohol, 15.5 min; oleoyl alcohol, 14 min. H_2O_2 was determined spectrophotometrically at 650 nm by using horseradish peroxidase to oxidize the chromogenic dye 2,2′-azino-bis(3-ethylbenzthiazoline-6-sulfonic acid).

RESULTS

Although steady-state kinetic studies have been performed on the acyl-ACP desaturases (*15*), comparable studies of

[2] An MCD study of 4e$^-$ Δ9D and the 18:0-ACP complex of 4e$^-$ Δ9D revealed substantial changes in the diiron center upon complex formation that are consistent with both diiron centers containing five-coordinate sites in 4e$^-$ Δ9D and both diiron centers containing one four-coordinate and one five-coordinate site in the complex (Y. Yang, J.A.B., B.G.F., and E. I. Solomon, manuscript submitted for publication).

Table 1: Rates of Reoxidation for Diiron Enzymes in the Presence of Various Substances

enzyme and substance	product	rate (min^{-1})
autoxidation[a]		
$4e^-$ reduced Δ9D alone[b]		<0.002
+ pantotheinate, CoA		<0.002
+ methyl stearate		<0.002
+ apo-ACP, holo-ACP		<0.002
+ 18:0-ACP	18:0-ACP, 2 H_2O	0.027
RNR R2 Y122F[c]		~10
MMOH alone[d]		1.3
+ component B		3.0
catalytic oxidation[e]		
Δ9D + 18:0-ACP[f]	18:1-ACP, 2 H_2O	20−30
RNR R2 Y122[c]	Y122•	42−60
MMOH + component B, CH_4[d]	CH_3OH	10.2

[a] Rate for reappearance of the resting enzyme in the absence of a natural substrate. [b] Autoxidation monitored by the appearance of the μ−oxo charge transfer band at 350 nm after addition of the appropriate compound to chemically reduced Δ9D exposed to 1 atm O_2. [c] Rate for conversion of the indicated RNR R2 isoforms to the diferric state (*42*, *43*). [d] Rate for conversion of reduced MMOH to diferric MMOH in the absence or presence of component B and methane (*24*). [e] Rate of catalytic oxidation leading to the formation of the standard product: for Δ9D, 18:1−ACP; for RNR R2, Y122•; for MMOH, CH_3OH. [f] Turnover number calculated from Δ9D multiple turnover at V_{max} in the presence of NADPH, ferredoxin reductase, *Anabaena* [2Fe-2S] ferredoxin, and 18:0−ACP.

single turnover catalysis have not been reported. In part, this arises from the difficulty in preparing sufficient quantities of 18:0-ACP to support these material-intensive experiments (*40*, *41*). However, our recent efforts to produce recombinant 18:0-ACP (*23*) have permitted the present examination of the single turnover reactivity of $4e^-$ reduced Δ9D ($4e^-$ Δ9D).

Comparison of Rates for Autoxidation and Catalytic Turnover. The single turnover autoxidation of $4e^-$ Δ9D was determined from reappearance of the 350 nm absorption band arising from oxo-bridged diferric centers (*4*). The conversion to the ferric state was slow (Table 1, $k' < 0.002$ min^{-1}) and was not affected by the addition of ~10^2−10^3-fold molar excess of pantotheinate, coenzyme A, methyl stearate, apo-ACP, or holo-ACP (Table 1), revealing that neither substrate analogues nor the protein portion of the natural substrate was able to influence the reactivity of $4e^-$ Δ9D. Likewise, the reoxidation rate was not changed in the pH range 6−9 and was not significantly increased at 40 °C. Upon completion of the autoxidation, >95% of the intensity of the original 340 nm absorption band was observed, suggesting near-stoichiometric recovery of diiron centers in the diferric state.

For diferrous RNR R2, Table 1 shows that the overall rate for single turnover oxidation of the natural isoform Y122 is 42−60 min^{-1} (*42*), while in RNR R2 isoform Y122F, representing an enzyme form lacking the residue that is the single turnover oxidation substrate, the rate of the autoxidation is ~10 min^{-1} (*43*). Thus, despite the large difference in the stability of tyrosine and phenylalanine to oxidation, and despite the difference in the ultimate products of the reaction, the reoxidation rates for RNR R2 isoforms Y122 and Y122F differ by only 6-fold (Table 1). In the case of chemically reduced MMOH, Table 1 shows that the rate of autoxidation in the absence of the component B effector protein and substrate is 1.3 min^{-1} (*44*), while the multiple turnover catalytic rate is increased by only ~10-fold to 10.2 min^{-1} upon addition of a suitable combination of the component B effector protein and methane (*24*, *44*).

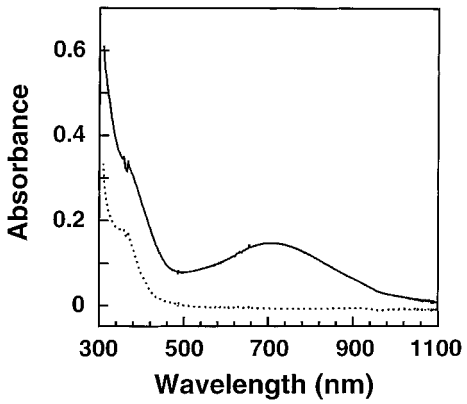

FIGURE 1: Optical spectra of $4e^-$ reduced stearoyl-ACP Δ^9 desaturase exposed to 1 atm of O_2 gas in the presence (solid line) or absence (dotted line) of 18:0-ACP.

In the absence of substrate, $4e^-$ Δ9D has an ~10^4 slower rate for single turnover autoxidation than RNR R2, RNR R2 Y122F, or MMOH (Table 1). Moreover, although the rate of reoxidation observed from $4e^-$ Δ9D in the presence of 18:0-ACP was increased by ~10-fold (Table 1, $k' \approx 0.027$ min^{-1}) as compared to $4e^-$ Δ9D alone, this rate is still 10^3-fold slower than that expected from the rate determined for catalytic desaturation (Table 1, $k' \approx 20-30$ min^{-1}). These behaviors are remarkably distinct from RNR R2 and MMOH and suggest unanticipated mechanisms for control of the Δ9D catalytic cycle.

Peroxodiferric Intermediate in Autoxidation. Resting Δ9D has absorption bands at 320 and 340 nm that are typical for oxo → Fe(III) charge transfer, whereas $4e^-$ Δ9D has no optical absorption in the visible region (*4*). The dotted line in Figure 1 shows the optical spectrum of $4e^-$ Δ9D exposed to O_2 gas (1 atm) in the absence of 18:0-ACP. No evidence for the formation of intermediates in the slow autoxidation was observed. Furthermore, no changes in absorption or autoxidation rate were observed if either apo-ACP (10-fold molar excess, lacking the functionally essential phosphopantetheine group) or holo-ACP (10-fold molar excess, lacking an acyl chain) were added to the reduced enzyme exposed to 1 atm O_2. However, when 18:0-ACP was added, a chromophoric complex with a broad absorption band at 700 nm and a shoulder at 380 nm was formed (solid line in Figure 1). The intensity of the 700 nm band was dependent on the concentration of $4e^-$ Δ9D present and could be increased by titration of 18:0-ACP into the reaction cuvette (see below). Other experiments revealed that the same optical spectrum was formed regardless of whether 18:0-ACP was added before or after reduction or before or after addition of O_2.

Figure 2 shows RR spectra obtained by 647.1 nm excitation of Δ9D samples prepared with $^{16}O_2$, $^{16}O^{18}O$ (50% isotopic enrichment), and $^{18}O_2$. When the O_2 adduct of the complex of $4e^-$ Δ9D and 18:0-ACP was formed in $^{16}O_2$, two features were observed at low frequency (442 and 490 cm^{-1}) that have the expected energy for ν_s and ν_{as} of an Fe−O_2 bond, while another feature was observed at high frequency (898 cm^{-1}) that has the expected energy for ν-(O−O) of a metal-coordinated peroxide (*26*, *45*, *46*). Each of the three vibrational bands observed in the $^{16}O_2$ samples

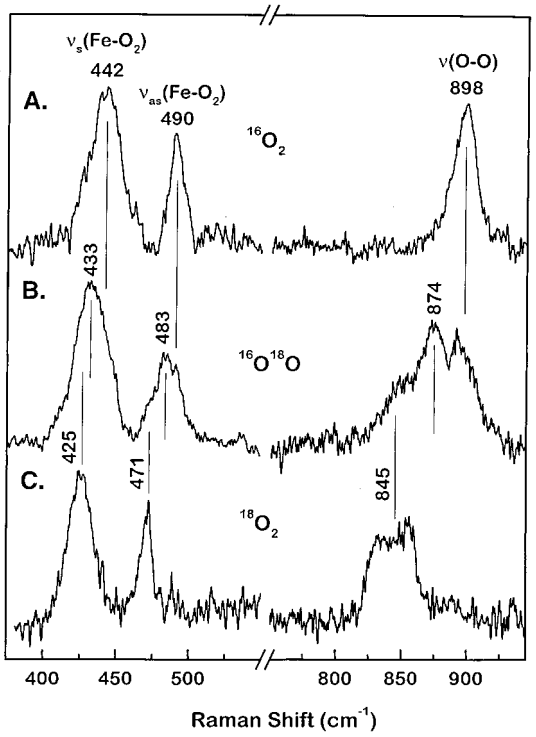

FIGURE 2: RR spectra of peroxodiferric Δ9D generated with (A) $^{16}O_2$, (B) $^{16}O^{18}O$ (50 atom % ^{18}O), and (C) $^{18}O_2$ (98 atom % ^{18}O). Each spectrum was obtained within 10 min after thawing and was corrected for protein peaks by subtracting the 10 min spectrum obtained 50 min after thawing. The peroxo intermediate essentially disappeared after the first 10 min due to photodecomposition in the laser beam.

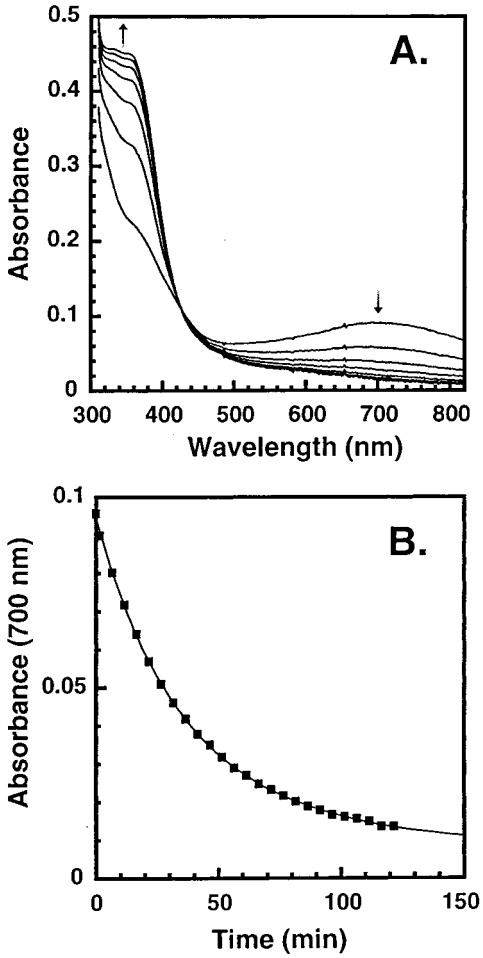

FIGURE 3: Decomposition of peroxodiferric Δ9D formed from Δ9D (43 μM holoprotein) and 18:0-ACP (140 μM). (A) Optical spectra obtained at 40 min intervals. The decrease in absorption at 700 nm and the increase in absorption at 340 nm are as indicated. (B) The time course of the absorbance change at 700 nm. The solid line is a nonlinear least-squares fit assuming single-exponential decay of peroxodiferric Δ9D.

were symmetric, single peaks. In a sample prepared with $^{18}O_2$, the low-frequency vibrational bands were shifted by −17 and −19 cm^{-1} to 425 and 471 cm^{-1}, respectively, while the high-frequency band was shifted by −54 to 845 cm^{-1}. The magnitudes of the observed frequency shifts were consistent with the change in mass expected for substitution of isotopically labeled O_2 into the chromophore. The low-frequency peaks in the $^{18}O_2$ sample were also clearly symmetric, single peaks, whereas the ν(O−O) band appeared to be a doublet. However, since ν(O−O) for the $^{16}O_2$-adduct was a single peak (898 cm^{-1}), the doublet centered at 845 cm^{-1} in the $^{18}O_2$ sample most likely arose from Fermi resonance with an unidentified mode not normally enhanced at this excitation wavelength. Fermi resonance has been previously observed in the RR spectra of other peroxodiferric model complexes (*47*) and in the $^{17}O_2$ complex of RNR R2 W48F/D84E, reported in the previous paper in this issue (*26*).

In the Δ9D sample prepared with $^{16}O^{18}O$, containing a 1:2:1 mixture of $^{16}O_2$, $^{16}O^{18}O$, and $^{18}O_2$, the center of the low-frequency vibrational bands appeared at 433 and 483 cm^{-1}, respectively, while the center of the high-frequency band appeared at 874 cm^{-1}. For each vibrational band, the frequency was nearly halfway between the frequencies observed in the $^{16}O_2$ and $^{18}O_2$ samples, which was consistent with partial change in mass. Furthermore, the use of $^{16}O^{18}O$ resulted in the resolution of all three vibrational bands [ν_s-(Fe−O), ν_{as}(Fe−O), ν(O−O)] into triplet vibrational peaks. Thus, for example, the ν(O−O) peak in the mixed isotope sample had a central component at 874 cm^{-1} and side components at 845 and 898 cm^{-1} whose intensities corresponded to the fractions of $^{16}O^{18}O$ (50%), $^{18}O_2$ (25%), and $^{16}O_2$ (25%) present in the gas, respectively. The presence of this triplet effectively ruled out asymmetric binding modes such as η^1 or μ-1,1, where two sets of triplets with vibrational frequencies characteristic of either ^{16}O- or ^{18}O-coordination to the metal center would be expected. Furthermore, the observed ν(O−O) was considerably higher than that observed for μ-η^2:η^2 peroxodicopper(II) complexes or oxyhemocyanin [∼750 cm^{-1} (*45*, *48*)]. Therefore, the vibrational spectra of Figure 2 are most consistent with a symmetric μ-1,2 peroxy structure in Δ9D,[3] which also establishes the fundamental structural similarity of the peroxy level intermediates in the two closely related diiron enzymes, Δ9D and RNR R2 W48F/D84E.

Decay of Peroxodiferric Δ9D. Figure 3A shows optical spectra obtained during the decay of peroxodiferric Δ9D, while Figure 3B shows the time course of the change in optical absorbance at 700 nm. During the decay, the loss of the 700 nm band corresponding to peroxodiferric Δ9D and the reappearance of the oxo → Fe(III) charge-transfer

[3] The cis-μ-1,2 and gauche-μ-1,2 configurations cannot be distinguished by vibrational data at present.

bands were associated with a reasonably tight isosbestic point at ~420 nm. After accounting for a nonzero A_∞ using Kedzy−Swinbourne analysis, plots of $\ln[(A(t) - A_\infty/A(0) - A_\infty)]$ versus time were linear for the complete decay process. Thus, the decrease in absorption at 700 nm was well fit with a single exponential, and nonlinear least-squares fitting of the experimental data gave $k_{app} = 0.027$ min^{-1}. The stability of peroxodiferric Δ9D was not dependent on the presence of O_2 as replacement of the headspace in the optical cuvette by repeated cycles of flushing with O_2-free Ar caused no change in the decay rate. Furthermore, the rate was independent of Δ9D concentration over a 4-fold range (20−80 μM), suggesting that intramolecular 2e$^-$ transfer was associated with the loss of the 700 nm absorption and return of the enzyme to the resting state.

Gas chromatographic analysis revealed that 18:1-ACP was not produced by the decay of peroxodiferric Δ9D, while the stearoyl chain was quantitatively recovered from total 18:0-ACP (>90%). For these catalytic assays, the detection limit for an oleoyl product relative to Δ9D active sites present was less than 0.5%. Likewise, a spectrophotometric assay for H_2O_2 release based on horseradish peroxidase-catalyzed dye oxidation revealed that no H_2O_2 was released during decay of peroxodiferric Δ9D. In similar assays, exogenously added H_2O_2 was quantitatively recovered at less than 5% of the molar amount of Δ9D active sites present. After the reoxidation was complete, an optical spectrum with nearly identical intensity to that of the original resting Δ9D preparation was obtained. This reoxidation cycle was repeated for three cycles with no loss in the ability to reform peroxodiferric Δ9D and with no decrease in the intensity of the resting oxo → Fe(III) charge-transfer band. Furthermore, redox-cycled Δ9D had multiple turnover activity ($k' \approx 20-30$ min^{-1} for 18:1-ACP production, Table 1) indistinguishable from the activity of aliquots of the same Δ9D preparation not subjected to the single turnover reoxidation cycle.

Stoichiometry of 18:0-ACP in the Peroxo Intermediate. Figure 4A shows a titration of 18:0-ACP into a solution of 4e$^-$ Δ9D equilibrated with 1 atm O_2. Due to the stability of 4e$^-$ Δ9D in the presence of O_2, and due to the relative stability of peroxodiferric Δ9D once formed, this titration was performed at 20 °C over ~6 min. Addition of 18:0-ACP aliquots caused the progressive appearance of the 700 and 380 nm absorption bands assigned to peroxodiferric Δ9D. The formation of this product was maximized after the addition of ~2 mol of 18:0-ACP/mol of Δ9D (Figure 4B), suggesting that one 18:0-ACP was bound per subunit of 4e$^-$ Δ9D. Other experiments performed by rapid addition of up to a 10-fold excess of 18:0-ACP revealed that no additional intensity of the 700 nm band could be formed. On the basis of the linear increase in absorption observed during the titration, a molar absorptivity of 1200 ± 50 M^{-1} cm^{-1} was determined relative to the concentration of 18:0-ACP added. While this value is similar to those determined for other peroxodiferric intermediates, RNR R2 D84E [~1500 M^{-1} cm^{-1} (*25*)], MMOH [~1500 M^{-1} cm^{-1} (*27*)], and crystallographically characterized synthetic model complexes [~1500−3540 M^{-1} cm^{-1} (*46*, *49*)], it does not conclusively reveal whether one or two peroxo moieties are present.

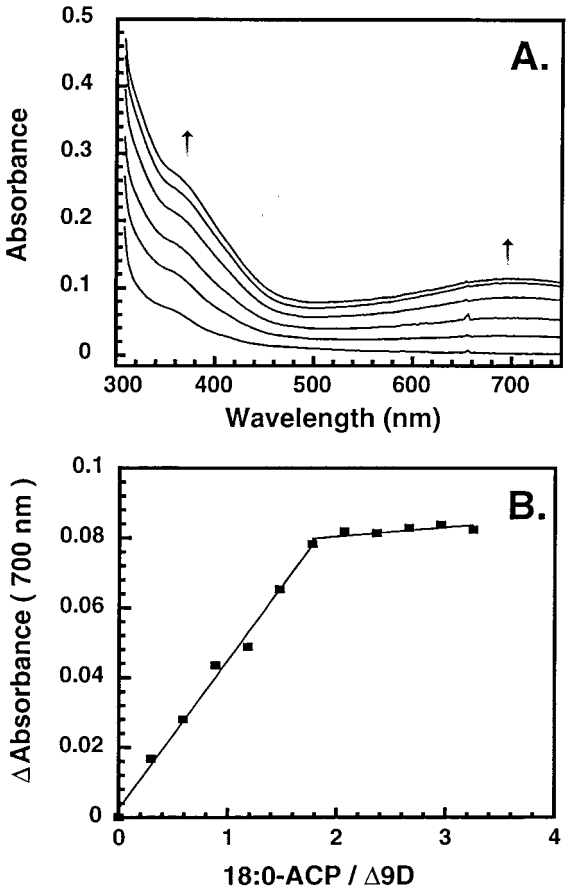

FIGURE 4: Formation of peroxodiferric Δ9D during titration with 18:0-ACP. (A) optical spectra obtained from successive addition of 5 μL aliquots of 1.23 mM 18:0-ACP to 4e$^-$ Δ9D (40 μM holoprotein). (B) The increase in absorbance at 700 nm plotted as a function of moles of 18:0-ACP added per mole of Δ9D dimer.

DISCUSSION

Many new insights into biological O_2 activation have been provided by study of RNR R2, MMOH, and synthetic active-site mimics (*50*). Since RNR R2, MMOH, and Δ9D have similar protein folds, ligation environments, and hydrophobic active sites, it is generally assumed that many aspects of their catalytic cycles will be closely related (*2*, *50*, *51*). This assumption has been validated by the similar Mössbauer properties of the peroxodiferric intermediates of RNR R2 D84E (*25*), MMOH compound P (H_{peroxo}) (*27*), and ferritin (*13*) and the similar Mössbauer properties of intermediate X of RNR R2 (*52*) and 1e$^-$ reduced MMOH compound Q (*31*). In combination with the previous study of RNR R2 W48F/D84E (*26*), this overall structural similarity has been refined to include symmetric μ-1,2 peroxodiferric intermediates in two of the three members of the class II diiron enzymes by use of vibrational spectroscopy.[4] However, these studies also reveal an unanticipated reactivity of 4e$^-$ Δ9D.

Structural Evidence for Peroxodiferric Δ9D. The addition of O_2 to the complex of 18:0-ACP and 4e$^-$ Δ9D results in the formation of a quasi-stable intermediate with a broad

[4] A resonance Raman feature initially ascribed to the putative peroxodiferric intermediate in MMOH (*53*) was later reported (*54*) to be an artifact arising, in part, from difficulties in the subtraction of the spectrum of 2-methylbutane cryosolvent used to prepare the freeze-quenched samples.

absorption maximum at 700 nm. When compared to oxyhemerythrin [ν(O−O) = 844 cm^{-1} for η^1 coordination (*55*)] or oxyhemocyanin [ν(O−O) = ∼750 cm^{-1} for μ-η^2:η^2 coordination (*45, 48*)], the relatively high ν(O−O) value of 898 cm^{-1} observed for peroxodiferric Δ9D is indicative of a bridging peroxide structure (*56*), as is the observation of two ν(Fe−O_2) modes at 442 and 490 cm^{-1}. Furthermore, the accompanying paper on the peroxodiferric intermediate of RNR R2 W48F/D84E reveals a remarkably similar RR spectrum with ν(O−O) at 870 cm^{-1}, ν_s(Fe−O_2) at 458 cm^{-1}, and ν_{as}(Fe−O_2) at 499 cm^{-1} (*26*). For both enzymes, the observation that the $^{16}O^{18}O$ mixed isotope produces single vibrational peaks split in a 1:2:1 pattern arising from the isotopic composition of the gas strongly supports our proposal that peroxide is coordinated to the class II diiron enzymes in a symmetric fashion, such as a μ-1,2 structure. This proposal is also consistent with the ability of azide to coordinate to resting Δ9D to form a μ-1,3 azidodiferric structure (*18*).

Functional Properties of Peroxodiferric Δ9D. Despite the structural similarities of the peroxodiferric intermediates detected in Δ9D and RNR R2, the functional properties of these two species differ significantly. For example, peroxodiferric RNR R2 D84E accumulates in air-saturated buffer and then decays with $t_{1/2}$ of ∼6 s to give the expected oxidation product Y122• (*25*), while peroxodiferric RNR R2 W48F/D84E is more stable by ∼4-fold and decays to generate a small amount of Y122• (*26*). In contrast, peroxodiferric Δ9D accumulates to high levels, but only when 4e$^-$ Δ9D, 18:0-ACP, and 1 atm O_2 are present: omission of 18:0-ACP or the substitution of air-saturated buffer does not support formation of this peroxy intermediate. The titration data of Figure 4 indicate that 18:0-ACP binds tightly to 4e$^-$ Δ9D, that 18:0-ACP binding linearly correlates with formation of the peroxy intermediate, and that each subunit of the Δ9D dimer can bind a substrate molecule. Peroxodiferric Δ9D then decays by a first-order process with $t_{1/2}$ of ∼26 min without detectable desaturation of 18:0-ACP, but likewise without detectable release of H_2O_2. This decay yields resting Δ9D in essentially quantitative recovery with respect to diferric centers as judged by optical spectroscopy and with respect to catalytic activity as judged by subsequent 18:1-ACP production using the enzymatic electron-transfer chain.

It is generally concluded that flexibility of the diiron center ligation environment has a major impact on catalysis (*10, 18*−*23*). In this regard, the stability of the peroxodiferric intermediate described here may arise from only relatively minor alterations in conformation associated with inappropriate redox state, ligation pattern, or Fe−Fe distance. The elucidation of how, or if, these alterations permit stable intermediates to be converted into more reactive states will likely provide further insight into O_2 activation by diiron centers.

Oxidase Chemistry of 4e$^-$ Δ9D. Chemically reduced Δ9D (containing 4e$^-$ in two diferrous sites) has a 10^4-fold lower reactivity with O_2 than either RNR R2 or MMOH, suggesting that Δ9D has a unique mechanism to prevent autoxidation. Moreover, 4e$^-$ Δ9D has ∼10^3-fold lower reactivity with O_2 in the presence of 18:0-ACP than enzymatically reduced Δ9D (possibly containing one diferrous cluster and one diferric cluster within the same dimeric protein, since a mixed valence state has not been observed). These observations suggest that the overall redox state of Δ9D may be an important determinant of the outcome of catalysis. Figure 5 shows proposed models accounting for the differences in catalytic properties of chemically reduced and enzymatically reduced Δ9D. We propose that 4e$^-$ chemical reduction of Δ9D produces a conformation that enforces oxidase chemistry (Figure 5A). The oxidase reaction occurs via the formation of an enzyme-bound peroxodiferric species and ultimately leads to recovery of resting Δ9D. In these experiments, diferrous centers are the only likely source of reducing equivalents.[5] Thus, the in vitro oxidase reaction may involve an intramolecular electron transfer between diferrous and peroxodiferric centers in different subunits of the enzyme (*60*). In principle, the 2e$^-$ reduction of either a peroxodiferric center or a high valent intermediate produced by homolysis

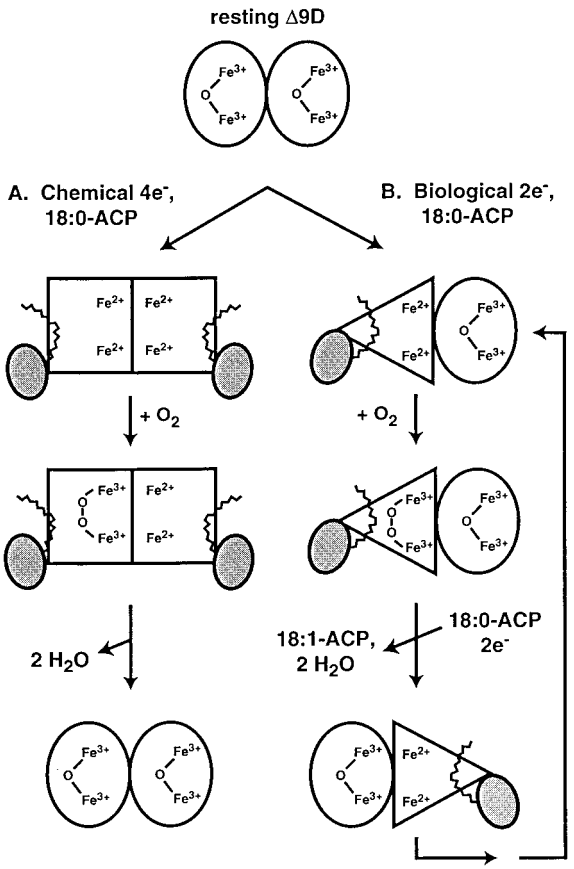

FIGURE 5: Oxidase and desaturase pathways of Δ9D differentiated by the overall redox state. (A) oxidase pathway initiated by 4e$^-$ chemical reduction. The origin of the oxo bridge (O_2 or solvent) in the resting enzyme produced after the oxidase reaction is not specified. (B) multiple turnover desaturation pathway initiated by 2e$^-$ enzymatic reduction of one diiron center of the dimeric resting enzyme. The use of alternating active sites is hypothesized to coordinate the transfer of reducing equivalents, substrate binding (18:0-ACP and O_2), and product release (18:1-ACP). The kinetic order of addition of reducing equivalents and substrates is not known.

[5] The 700 nm band was quickly lost upon addition of either sodium dithionite or reduced [2Fe-2S] ferredoxin, and resulted in the reappearance of the oxo → Fe(III) charge-transfer band of resting Δ9D (J.A.B. and B.G.F., unpublished results). Therefore, an alternative electron-transfer pathway related to that proposed for residue W48 of RNR R2 (*9, 57*−*59*) may also be present in Δ9D, which has a structurally analogous tryptophan, W62.

of the O−O bond in the peroxodiferric center are possible mechanisms to restore resting Δ9D. These options cannot be distinguished at present.

Mechanistic Implications of Oxidase versus Desaturase Reactions. The observation that the oxidase reaction occurs on $4e^-$ Δ9D, but that acyl-ACP desaturation does not, implies that multiple turnover catalysis may normally proceed via a "half-site" reactivity (Figure 5B), which has also been described for RNR R2 (*61*). Presently, the kinetic order for addition of reducing equivalents, O_2 and 18:0-ACP, and for the release of 18:1-ACP is not known for Δ9D. Likewise, a peroxodiferric intermediate has not been established for desaturase catalysis, but remains an attractive possibility. One possible advantage of the redox-cycle gated process summarized in Figure 5B would be that 18:0-ACP binding to the unreacted subunit could be coordinated with 18:1-ACP release from the other subunit. Furthermore, these conformational changes may be associated with activation of various O_2 adducts during the catalytic cycle. We postulate that a complete loading of electrons and 18:0-ACP onto the Δ9D dimer by chemical reduction may disrupt this cycle, thus allowing for the observed oxidase chemistry.

Biological Implications of the Oxidase Reaction. Although the autoxidation of $4e^-$ Δ9D in the presence of 18:0-ACP is $\sim 10^3$-fold slower than the desaturation of 18:0-ACP by biologically reduced Δ9D, this autoxidation chemistry provides a route to restore resting Δ9D without yielding deleterious products such as H_2O_2. Since Δ9D is found in long-lived organelles such as the chloroplast and plastid, which also contain substantial levels of reducing equivalents, evolutionary selection may have provided Δ9D a control of diiron center reactivity that has not been necessary in RNR R2 and MMOH, which are both from more rapidly growing bacteria.

Δ9D appears to be able to perform oxidase chemistry using $4e^-$ entirely from diiron centers without oxidation of active-site amino acids. In contrast, RNR R2 performs an oxidase reaction using $2e^-$ from a diferrous center, $1e^-$ from Y122, and $1e^-$ from an exogenous source. MMOH from *Methylococcus capsulatus* (Bath) has also been proposed to convert between hydroxylase and oxidase activities as a function of component B (*62*). This process is of obvious relevance to the oxidase reactivity reported here, however, no enzyme intermediates were detected during these previous studies.

The $4e^-$ reduction of O_2 to $2H_2O$ without acyl desaturation and without H_2O_2 release described here represents a new mode of catalysis for Δ9D that is further supported by the identification of a key intermediate in the reaction. This demonstration of oxidase catalysis is consistent with the rapid increase in the number of functions reported for diiron enzymes in the past few years (*51*, *63*). In this regard, the "alternative oxidase" from fungi, plants, and trypanosomes has recently been proposed to be a diiron enzyme having repeats of the sequence motif GluXXHis (*6*, *64*−*66*). Although further studies, including confirmation of the metal binding motif and the verification of a spin-coupled iron environment, are required, the catalytic and spectroscopic properties reported here for single turnover preparations of $4e^-$ Δ9D may indeed provide a mechanistic framework for further investigation of the "alternative oxidase" reaction by the putative membrane diiron centers.

ACKNOWLEDGMENT

We thank Dr. Rolf Thauer for an enthusiastic discussion of the mechanism of half-site reactivity and Dr. John Shanklin for the expression vector for acyl-ACP synthase-His_6.

REFERENCES

1. Feig, A., and Lippard, S. J. (1994) *Chem. Rev. 94*, 759−805.
2. Wallar, B. J., and Lipscomb, J. D. (1996) *Chem. Rev. 96*, 2625−2657.
3. Fox, B. G. (1997) in *Comprehensive Biological Catalysis* (Sinnott, M., Ed.) pp 261−348, Academic Press, London.
4. Fox, B. G., Shanklin, J., Ai, J., Loehr, T. M., and Sanders-Loehr, J. (1994) *Biochemistry 33*, 12776−12786.
5. Shanklin, J., Whittle, E., and Fox, B. G. (1994) *Biochemistry 33*, 12787−12794.
6. Moore, A. L., Umbach, A. L., and Siedow, J. N. (1995) *J. Bioeng. Biomembr. 27*, 367−377.
7. Harrison, P., and Arosio, P. (1996) *Biochim. Biophys. Acta 1275*, 161−203.
8. deMaré, F., Kurtz, D. M., and Nordlund, P. (1996) *Nat. Struct. Biol. 3*, 539−546.
9. Nordlund, P., and Eklund, H. (1993) *J. Mol. Biol. 232*, 123−164.
10. Rosenzweig, A. C., Nordlund, P., Takahara, P. M., Frederick, C. A., and Lippard, S. J. (1995) *Chem. Biol. 2*, 409−418.
11. Elango, N., Radhakrishnan, R., Froland, W. A., Wallar, B. J., Earhart, C. A., Lipscomb, J. D., and Ohlendorf, D. H. (1997) *Protein Sci. 6*, 556−568.
12. Lindqvist, Y., Huang, W., Schneider, G., and Shanklin, J. (1996) *EMBO J. 15*, 4081−4092.
13. Pereira, A. S., Small, W., Krebs, C., Tavares, P., Edmondson, D. E., Theil, E. C., and Huynh, B. H. (1998) *Biochemistry 37*, 9871−9876.
14. Bonomi, F., Kurtz, D. M., Jr., and Cui, X. (1996) *J. Biol. Inorg. Chem. 1*, 67−72.
15. Shanklin, J., and Cahoon, E. B. (1998) *Annu. Rev. Plant Physiol. Plant Mol. Biol. 49*, 611−641.
16. Fox, B. G., Shanklin, J., Somerville, C., and Münck, E. (1993) *Proc. Natl. Acad. Sci. U.S.A. 90*, 2486−2490.
17. Shu, L., Broadwater, J. A., Achim, C., Fox, B. G., Münck, E., and Que, L., Jr. (1998) *J. Biol. Inorg. Chem. 3*, 392−400.
18. Ai, J., Broadwater, J. A., Loehr, T. M., Sanders-Loehr, J., and Fox, B. G. (1997) *J. Biol. Inorg. Chem. 2*, 37−45.
19. Logan, D. T., Su, X.-D., Åberg, A., Regnström, K., Hajdu, J., Eklund, H., and Nordlund, P. (1996) *Structure 4*, 1053−1064.
20. Rardin, R. L., Tolman, W. B., and Lippard, S. J. (1991) *New J. Chem. 15*, 417−430.
21. Shu, L., Nesheim, J. C., Kauffmann, K., Münck, E., Lipscomb, J. D., and Que, L., Jr. (1997) *Science 275*, 515−518.
22. Shu, L., Liu, Y., Lipscomb, J. D., and Que, L., Jr. (1996) *J. Biol. Inorg. Chem. 1*, 297−304.
23. Broadwater, J. A., Haas, J. A., and Fox, B. G. (1998) *FETT/Lipid 100*, 103−113.
24. Lee, S.-K., Nesheim, J. C., and Lipscomb, J. D. (1993) *J. Biol. Chem. 268*, 21569−21577.
25. Bollinger, J. M., Jr., Krebs, C., Vicol, A., Chen, S., Ley, B. A., Edmondson, D. E., and Huynh, B. H. (1998) *J. Am. Chem. Soc. 120*, 1094−1095.
26. Moënne-Loccoz, P., Baldwin, J., Ley, B. A., Loehr, T., and Bollinger, J. M., Jr. (1998) *Biochemistry 37*, 14659−14663.
27. Liu, K. E., Valentine, A. M., Wang, D., Huynh, B. H., Edmondson, D. E., Salifoglou, A., and Lippard, S. J. (1995) *J. Am. Chem. Soc. 117*, 10174−10185.
28. Lee, S.-K., Fox, B. G., Froland, W. F., Lipscomb, J. D., and Münck, E. (1993) *J. Am. Chem. Soc. 115*, 6450−6451.
29. Sturgeon, B. E., Burdi, D., Chen, S., Huynh, B.-H., Edmondson, D. E., Stubbe, J., and Hoffman, B. M. (1996) *J. Am. Chem. Soc. 118*, 7551−7557.
30. Willems, J.-P., Lee, H.-I., Burdi, D., Doan, P. E., Stubbe, J., and Hoffman, B. M. (1997) *J. Am. Chem. Soc. 119*, 9816−9824.

31. Valentine, A. M., Tavares, P., Pereria, A. S., Davydov, R., Krebs, C., Hoffman, B. M., Edmondson, D. E., Huynh, B. H., and Lippard, S. J. (1998) *J. Am. Chem. Soc. 120*, 2190−2191.
32. Riggs-Gelasco, P. J., Shu, L., Chen, S., Burdi, D., Huynh, B. H., Que, L., Jr., and Stubbe, J. (1998) *J. Am. Chem. Soc. 120*, 849−860.
33. Hoffman, B. J., Broadwater, J. A., Johnson, P., Harper, J., Fox, B. G., and Kenealy, W. R. (1995) *Protein Expression Purif. 6*, 646−654.
34. Bradford, M. M. (1976) *Anal. Biochem. 72*, 248−252.
35. Fischer, D. S., and Price, D. C. (1964) *Clin. Chem. 10*, 21−30.
36. Lambalot, R. H., and Walsh, C. T. (1995) *J. Biol. Chem. 270*, 24658−24661.
37. Rock, C. O., and Garwin, J. L. (1979) *J. Biol. Chem. 254*, 7123−7128.
38. Espenson, J. H. (1981) in *Chemical Kinetics and Reaction Mechanisms*, McGraw-Hill, New York, p 218.
39. Barron, E. J., and Mooney, L. A. (1968) *Anal. Chem. 40*, 1742−1744.
40. Beremand, P. D., Hannapel, D. J., Guerra, D. J., Kuhn, D. N., and Ohlrogge, J. B. (1987) *Arch. Biochem. Biophys. 256*, 90−100.
41. Hill, R. B., MacKenzie, K. R., Flanagan, J. M., Cronan, J. E., Jr., and Prestegard, J. H. (1995) *Protein Expression Purif. 6*, 394−400.
42. Tong, W. H., Chen, S., Lloyd, S. G., Edmondson, D. E., Huynh, B.-H., and Stubbe, J. (1996) *J. Am. Chem. Soc. 118*, 2107−2108.
43. Sahlin, M., Lassmann, G., Pötsch, S., Sjöberg, B.-M., and Gräslund, A. (1995) *J. Biol. Chem. 270*, 12361−12372.
44. Liu, Y., Nesheim, J. C., Lee, S.-K., and Lipscomb, J. D. (1995) *J. Biol. Chem. 270*, 24662−24665.
45. Kitajima, N., Fujisawa, K., Fujimoto, C., Moro-oka, Y., Hashimoto, S., Kitagawa, T., Toriumi, K., Tatsumi, K., and Nakamura, A. (1992) *J. Am. Chem. Soc. 114*, 1277−1291.
46. Kim, K., and Lippard, S. J. (1996) *J. Am. Chem. Soc. 118*, 4914−4915.
47. Dong, Y., Ménage, S., Brennan, B. A., Elgren, T. E., Jang, H. G., Pearce, L. L., and Que, L., Jr. (1993) *J. Am. Chem. Soc. 115*, 1851−1859.
48. Freedman, T. B., Sanders-Loehr, J., and Loehr, T. (1978) *J. Am. Chem. Soc. 98*, 2809.
49. Kitajima, N., Tamura, N., Fukui, H., Moro-oka, Y., Mitzutani, Y., Kitagawa, T., Mathur, R., Heerwegh, K., Reed, C. A., Randall, C. R., Que, L., Jr., and Tatsumi, K. (1994) *J. Am. Chem. Soc. 116*, 9071−9085.
50. Que, L., Jr., and Dong, Y. (1996) *Acc. Chem. Res. 29*, 190−196.
51. Broadwater, J. A., Haas, J. A., Achim, C., Münck, E., Ai, J., Sanders-Loehr, J., Loehr, T. M., and Fox, B. G. Catalytic studies of acyl-ACP desaturation: The unique contributions of protein and lipid to enzymatic catalysis. Presented at the *26th Steenbock Symposium: Kinetics of Enzymatic Catalysis* (Frey, P. A., and Northrup, D., Eds.) May 28−31, 1998, Madison, WI, IOS Press, Amsterdam.
52. Ravi, N., Bollinger, J. M., Jr., Huynh, B. H., Edmondson, D. E., and Stubbe, J. (1994) *J. Am. Chem. Soc. 116*, 8007−8014.
53. Liu, K. E., Valentine, A. M., Qui, D., Edmondson, D. E., Appelman, E. H., Spiro, T. G., and Lippard, S. J. (1995) *J. Am. Chem. Soc. 117*, 4997−4998.
54. Liu, K. E., Valentine, A. M., Qui, D., Edmondson, D. E., Appelman, E. H., Spiro, T. G., and Lippard, S. J. (1997) *J. Am. Chem. Soc. 119*, 11134−11136.
55. Freier, S. M., Duff, L. I., Shriver, D. F., and Klotz, I. M. (1980) *Arch. Biochem. Biophys. 205*, 449−463.
56. Ross, P. K., and Solomon, E. I. (1991) *J. Am. Chem. Soc. 113*, 3246−3259.
57. Rova, U., Goodztzova, K., Ingemarson, R., Behravan, G., Gräslund, A., and Thelander, L. (1995) *Biochemistry 34*, 4267−4275.
58. Ekberg, M., Sahlin, M., Eriksson, M., and Sjöberg, B.-M. (1996) *J. Biol. Chem. 271*, 20655−20659.
59. Parkin, S. E., Chen, S., Ley, B. A., Mangravite, L., Edmondson, D. E., Huynh, B. H., and Bollinger, J. M., Jr. (1998) *Biochemistry 37*, 1124−1130.
60. Elgren, T. E., Lynch, J. B., Juarez-Garcia, C., Münck, E., Sjöberg, B.-M., and Que, L., Jr. (1991) *J. Biol. Chem. 266*, 19265−19268.
61. Sjöberg, B.-M., Karlsson, M., and Jörnvall, H. (1987) *J. Biol. Chem. 262*, 9736−9743.
62. Green, J., and Dalton, H. (1985) *J. Biol. Chem. 260*, 15795−15801.
63. Shanklin, J., Achim, C., Schmidt, H., Fox, B. G., and Münck, E. (1997) *Proc. Natl. Acad. Sci. U.S.A. 94*, 2981−2986.
64. Siedow, J. N., Umbach, A. L., and Moore, A. L. (1995) *FEBS Lett. 362*, 10−14.
65. Chaudhuri, M., and Hill, G. C. (1996) *Mol. Biochem. Parasitol. 83*, 125−129.
66. Chaudhuri, M., Ajayi, W., and Hill, G. C. (1998) *Mol. Biochem. Parasitol. 95*, 53−68.

BI981839I